ページ 1: [3] 書式変更	松下 健二	11/07/01 11:19

フォント:Times

ページ 1: [3] 書式変更	松下 健二	11/07/01 11:19

フォント:Times

ページ 1: [3] 書式変更	松下 健二	11/07/01 11:19

フォント:Times

ページ 1: [3] 書式変更	松下 健二	11/07/01 11:19

フォント:Times

ページ 1: [3] 書式変更	松下 健二	11/07/01 11:19

フォント:Times

ページ 1: [3] 書式変更	松下 健二	11/07/01 11:19

フォント:Times

ページ 1: [3] 書式変更	松下 健二	11/07/01 11:19

フォント:Times

ページ 1: [4] 書式変更	松下 健二	11/07/01 11:19

フォント:Times

ページ 1: [4] 書式変更	松下 健二	11/07/01 11:19

フォント:Times

ページ 1: [4] 書式変更	松下 健二	11/07/01 11:19

フォント:Times

ページ 1: [4] 書式変更	松下 健二	11/07/01 11:19

フォント:Times

ページ 1: [5] 書式変更	松下 健二	11/07/01 11:19

フォント:Times

ページ 1: [5] 書式変更	松下 健二	11/07/01 11:19

フォント:Times

ページ 1: [6] 削除	松下 健二	11/07/01 11:00

Flavonoids are a group of polyphenolic compounds, which have the diphenylpropane (C6–C3–C6) skeleton. Historically, the benzene ring is denoted 'A'-ring, the pyran ring 'C' ring, and the phenyl ring 'B'-ring. Flavonoids are a class of plant secondary metabolites and more than 8,000 different flavonoids have been described so far[1]. The flavonoid family includes flavones, flavonols, flavanones, flavanonols, flavans, flavanols, leucoanthocyanidins, anthocyanidins, aurones, chalcones, and isofavones. The structural difference in each flavonoid family results from the variation in the number and arrangement of the hydroxyl groups and the extent of glycosylation of these groups.

ページ 1: [6] 削除	松下 健二	11/07/01 11:00

Flavonoids are a group of polyphenolic compounds, which have the diphenylpropane (C6–C3–C6) skeleton. Historically, the benzene ring is denoted 'A'-ring, the pyran ring 'C' ring, and the phenyl ring 'B'-ring. Flavonoids are a class of plant secondary metabolites and more than 8,000 different flavonoids have been described so far[1]. The flavonoid family includes flavones, flavonols, flavanones, flavanonols, flavans, flavanols, leucoanthocyanidins, anthocyanidins, aurones, chalcones, and isofavones. The structural difference in each flavonoid family results from the variation in the number and arrangement of the hydroxyl groups and the extent of glycosylation of these groups.

ページ 1: [7] 削除	松下 健二	11/07/01 11:15

These endothelial adhesion molecules in turn facilitate the attachment of blood leukocytes to endothelial cell surfaces. [6]

ページ 2: [8] 書式変更	松下 健二	11/07/01 11:19

フォント:Times

ページ 2: [8] 書式変更	松下 健二	11/07/01 11:19

フォント:Times

ページ 2: [9] 削除	松下 健二	11/07/01 11:10

HUVEC (4 x 10^4 cells/well) were seeded into a 96-well microtiter plate and grown with EBM-2 overnight. The Medium was replaced by DMEM and then 10 ng/ml of TNF-α was added to each well with or without various concentrations of test specimens. After three hours, the medium was removed and the cell layer was washed 3 times with ice-cold PBS/1% BSA and fixed with 4% paraformaldehyde phosphate buffer. After being washed with PBS 5 times, the cells were incubated with PBS/1% BSA for 60 min. After being washed with PBS 3 times, the cells were incubated with an anti-E-selectin antibody at 4°C overnight (1:1,000 in PBS/1% BSA). After being washed with PBS 3 times, the AP-conjugated secondary antibody (1:500 in PBS/1% BSA) was added for 120 min. After the addition of p-nitrophenyl phosphate (pNPP) solution, the enzymatic reaction was allowed to proceed for 60 min at room temperature; the optical density (OD: 405 nm) was measured using the ELISA plate reader.

ページ 2: [10] 書式変更	松下 健二	11/07/01 11:19

フォント:Times

ページ 2: [10] 書式変更	松下 健二	11/07/01 11:19

フォント:Times

ページ 2: [10] 書式変更	松下 健二	11/07/01 11:19

フォント:Times

ページ 2: [10] 書式変更 松下 健二 11/07/01 11:19

フォント:Times

ページ 2: [10] 書式変更 松下 健二 11/07/01 11:19

フォント:Times

ページ 2: [10] 書式変更 松下 健二 11/07/01 11:19

フォント:Times

ページ 2: [10] 書式変更 松下 健二 11/07/01 11:19

フォント:Times

ページ 2: [10] 書式変更 松下 健二 11/07/01 11:19

フォント:Times

ページ 2: [10] 書式変更 松下 健二 11/07/01 11:19

フォント:Times

ページ 2: [10] 書式変更 松下 健二 11/07/01 11:19

フォント:Times

ページ 2: [10] 書式変更 松下 健二 11/07/01 11:19

フォント:Times

ページ 2: [10] 書式変更 松下 健二 11/07/01 11:19

フォント:Times

ページ 2: [10] 書式変更 松下 健二 11/07/01 11:19

フォント:Times

ページ 2: [10] 書式変更　松下 健二　11/07/01 11:19

フォント:Times

ページ 2: [10] 書式変更　松下 健二　11/07/01 11:19

フォント:Times

ページ 2: [10] 書式変更　松下 健二　11/07/01 11:19

フォント:Times

ページ 2: [10] 書式変更　松下 健二　11/07/01 11:19

フォント:Times

ページ 2: [10] 書式変更　松下 健二　11/07/01 11:19

フォント:Times

ページ 2: [10] 書式変更　松下 健二　11/07/01 11:19

フォント:Times

ページ 2: [10] 書式変更　松下 健二　11/07/01 11:19

フォント:Times

ページ 2: [10] 書式変更　松下 健二　11/07/01 11:19

フォント:Times

ページ 2: [10] 書式変更　松下 健二　11/07/01 11:19

フォント:Times

ページ 2: [10] 書式変更　松下 健二　11/07/01 11:19

フォント:Times

ページ 2: [10] 書式変更	松下 健二	11/07/01 11:19

フォント:Times

ページ 2: [11] 削除	松下 健二	11/07/01 11:13

Flavonoids may inhibit early events in the atherosclerotic process by modulating monocyte adhesion and transmigration. Although the mechanisms underlying the protection by flavonoids against the early atherogenic process are not fully understood, they may involve downregulation of inflammatory chemokines and cytokines, matrix proteases, and CAM [8, 9].

ページ 2: [12] 削除	松下 健二	11/07/01 11:00

Davide Grassi, Giovambattista Desideri ,Claudio Ferri,
Flavonoids:AntioxidantsAgainst
Atherosclerosis. Nutrients 2010, 2, 889-902

Okawa M, Kinjo J, Nohara T, et al: DDPH(1,1- -diphenyl-2-picrylhydrazyl) radical scavenging activity of flavonoids obtained from some medicinal plants.Biol Pharm Bull
2001, 24(10):1202-5.

ページ 2: [13] 書式変更	松下 健二	11/07/01 11:17

インデント: 左: 0 mm, ぶら下げインデント: 7.2 字, 1 行の文字数を指定時に右のインデント幅を自動調整する, 間隔段落前: 0 pt, 段落後: 0 pt, 改ページ時 1 行残して段落を区切る, 日本語と英字の間隔を自動調整する, 日本語と数字の間隔を自動調整する

ページ 2: [14] 削除	松下 健二	11/07/01 11:17

3. Chirumbolo S: The role of quercetin, flavonols and flavones in modulating inflammatory cell function. *Inflamm Allergy Drug Targets*, 9:263-285.
4. Dong ZM, Wagner DD: Leukocyte-endothelium adhesion molecules in

atherosclerosis. *J Lab Clin Med* 1998, 132:369-375.

5. Iiyama K, Hajra L, Iiyama M, Li H, DiChiara M, Medoff BD, Cybulsky MI: Patterns of vascular cell adhesion molecule-1 and intercellular adhesion molecule-1 expression in rabbit and mouse atherosclerotic lesions and at sites predisposed to lesion formation. *Circ Res* 1999, 85:199-207.
6. Osterud B, Bjorklid E: Role of monocytes in atherogenesis. *Physiol Rev* 2003, 83:1069-1112.
7. Ross R: Atherosclerosis--an inflammatory disease. *N Engl J Med* 1999, 340:115-126.
8. Aviram M, Fuhrman B: Wine flavonoids protect against LDL oxidation and atherosclerosis. *Ann N Y Acad Sci* 2002, 957:146-161.
9. Middleton E, Jr., Kandaswami C, Theoharides TC: The effects of plant flavonoids on mammalian cells: implications for inflammation, heart disease, and cancer. *Pharmacol Rev* 2000, 52:673-751

SHOCK, Vol. 36, No. 5, pp. 494–500, 2011

VALPROIC ACID INCREASES SUSCEPTIBILITY TO ENDOTOXIN SHOCK THROUGH ENHANCED RELEASE OF HIGH-MOBILITY GROUP BOX 1

Shinsuke Sugiura,*† Yuichi Ishihara,† Toshinori Komatsu,* Makoto Hagiwara,* Naomi Tanigawa,* Yoshiko Kato,*† Hiroki Mizutani,† Ko-ichi Kawahara,‡ Ikuro Maruyama,‡ Toshihide Noguchi,† and Kenji Matsushita*†

**Department of Oral Disease Research, National Center for Geriatrics and Gerontology, Obu; †Department of Periodontology, School of Dentistry, Aichi Gakuin University, Nagoya, Aichi; and ‡Department of Laboratory and Molecular Medicine, Shin Nippon Biomedical Laboratories Inc, Kagoshima University, Kagoshima, Japan*

Received 17 Mar 2011; first review completed 1 Apr 2011; accepted in final form 21 Jul 2011

ABSTRACT—High-mobility group box 1 (HMGB1) is a nuclear factor and a secreted protein. During inflammation, HMGB1 is secreted into the extracellular space where it can interact with the receptor for advanced glycation end products and trigger proinflammatory signals. Extracellular HMGB1 plays a critical role in several inflammatory diseases such as sepsis and rheumatoid arthritis. Valproic acid (VPA) is one of the most frequently prescribed antiepileptic drugs. The present study was undertaken to investigate the effect of VPA on secretion of HMGB1 in systemic inflammatory responses induced by lipopolysaccharide. Pretreatment with VPA increased the susceptibility of mice to lipopolysaccharide in endotoxemia. Valproic acid induced HMGB1 release and nuclear factor κB activation in RAW-blue cells. Valproic acid promoted the phosphorylation of ERK1/2 but not that of p38 or JNK. The MEK1/2 inhibitor PD98059 also suppressed HMGB1 release and activation of nuclear factor κB induced by VPA. Valproic acid induced expression of γ-aminobutyric acid receptors in macrophages, and picrotoxin, a γ-aminobutyric acid A receptor antagonist, inhibited the VPA-activated phosphorylation of ERK and VPA-induced HMGB1 release. These results suggest that VPA may exacerbate innate immune responses to endotoxin through enhanced release of HMGB1.

KEYWORDS—Sepsis, alarmin, lipopolysaccharide, histone deacetylases, inflammation, immunomodulation, cytokines

INTRODUCTION

Sequential cytokine induction by cells of the mononuclear phagocyte system has been found *in vitro* and *in vivo* following endotoxin stimulation. These cytokines, such as tumor necrosis factor (TNF), interleukin 6 (IL-6) and IL-1, are thought to be important as regulators of the immune system under physiologic conditions. However, excessive amounts of cytokines play a role in the pathologic manifestations of endotoxemia. High-mobility group box 1 (HMGB1), a protein previously known as a nuclear transcription factor, is a critical mediator of lethality in endotoxemia and sepsis (1). During a systemic inflammatory response, HMGB1 is released into the circulation by activated monocytes and by damaged cells. Administration of antibodies to HMGB1 attenuates endotoxin lethality in mice. Therefore, it is thought that HMGB1 is an important mediator of lethal systemic inflammation (1).

Inhibitors of nuclear histone deacetylases (HDACs) have been shown to suppress cancer cell proliferation *in vitro* (2, 3) and reduce experimental tumor growth *in vivo* (4, 5). Histone deacetylase inhibitors include short-chain fatty acids, hydroxamic acids, cyclic tetrapeptides, and benzamides. Suberyolanilide hydroxamid acid (SAHA)—the classic member of the class of hydroxamic acids—has potent anti-inflammatory activities, both *in vitro* and *in vivo* (6, 7). Histone deacetylase inhibition was shown to be associated with significant suppression of the production of proinflammatory cytokines (8, 9). These anti-inflammatory properties were confirmed by studies demonstrating that treatment with SAHA resulted in a significant reduction of disease severity in a murine model of systemic lupus erythematosus, the MLR-*lpr/lpr* mouse (10). The anti-inflammatory effects described for HDAC inhibitors have so far been limited to SAHA (11) and trichostatin A (TSA) (8, 12), both members of the class of hydroxamic acids. Thus, it remains to be clarified whether the anti-inflammatory effects of HDAC inhibition are restricted to this class or whether inhibition of HDACs in general results in suppression of cytokine production.

Many studies show that various HDAC inhibitors suppress inflammation. A few studies show that select HDAC inhibitors can increase inflammation. The differences between these results are probably explained by differences in the specificity of HDAC inhibitors and the various animal models used to uncover the mechanisms of inflammation.

Valproic acid (VPA) is an HDAC inhibitor of the class of short-chain fatty acids (13), and it is an established drug in the treatment of epileptic seizures and bipolar disorder (14). Accumulated experimental and clinical data also show that VPA might be a potent anticancer drug (15). Valproic acid also has anti-inflammatory effects (16). On the other hand, in some cases, VPA augments inflammatory responses; patients

Address reprint requests to Kenji Matsushita, DDS, PhD, Department of Oral Disease Research, National Center for Geriatrics and Gerontology, Obu, Aichi 4747-8511, Japan. E-mail: kmatsu30@ncgg.go.jp.

This work was supported by Grants-in-Aid for Scientific Research 22390354 and 21659436 (to K.M.) from the Ministry of Education, Culture, Sports, Science and Technology, Japan.

Supplemental digital content is available for this article. Direct URL citation appears in the printed text and is provided in the HTML and PDF versions of this article on the journal's Web site (www.shockjournal.com).

DOI: 10.1097/SHK.0b013e31822f7e58

receiving VPA may well develop hemorrhagic pancreatitis, bone marrow suppression, and hepatotoxicity (17, 18). Gingival overgrowth and progression of gingival inflammation are sometimes observed in patients who are taking VPA chronically (19). However, the mechanisms underlying the inflammatory effects of VPA are not known. In the present study, we found that VPA enhanced systemic inflammatory responses induced by lipopolysaccharide (LPS) by promoting the secretion of HMGB1 in murine macrophage cultures and in a murine model of endotoxic shock.

MATERIALS AND METHODS

Materials

Valproic acid and SAHA were purchased from Sigma-Aldrich (St Louis, Mo). Trichostatin A was purchased from Calbiochem (San Diego, Calif). *Escherichia coli* O18 LPS and TNF-α were purchased from Sigma-Aldrich. Purified rabbit polyclonal antibodies to HMGB1 and chicken polyclonal antibodies to HMGB1 were purchased from SHINO-TEST (Tokyo, Japan). Mouse monoclonal antibodies to phospho-ERK1/2, p38, and JNK were purchased from Cell Signaling Technology (Beverly, Mass). Mouse monoclonal antibodies to ERK1/2, p38, and JNK were purchased from BD Bioscience (Franklin Lakes, NJ). Mouse monoclonal antibodies to β-actin were purchased from BioVision (San Francisco, Calif).

Cell culture

RAW-blue cells were established from RAW 264.7 macrophage cells (InvivoGen, San Diego, Calif). They stably express a secreted embryonic alkaline phosphatase gene inducible by nuclear factor κB (NF-κB) and AP-1 transcription factors. RAW-blue cells were precultured in RPMI 1640 medium (Gibco BRL, Grand Island, NY) supplemented with 10% fetal bovine serum and 2 mM L-glutamine.

Analysis of HMGB1 release

To determine the effect of VPA on HMGB1 release, RAW-blue cells were stimulated with various concentrations of VPA, *E. coli* LPS, TNF-α, TSA, and SAHA, and the amount of HMGB1 released into the medium was measured by enzyme-linked immunosorbent assay (ELISA) (SHINO-TEST).

Measurement of NF-κB activity

RAW-blue cells were incubated with VPA. Culture supernatants of the cells were mixed with QUANTI-blue (InvivoGen), an alkaline phosphatase substrate, and then incubated for 30 min at 37°C. The absorbance (λ = 595 nm) was measured by using Appliskan (Thermo Fisher Scientific, Waltham, Mass) to detect relative NF-κB activity.

Western blotting

RAW-blue cells were incubated with various specimens for 0.5 to 24 h. Cells were lysed in Celytic M (Sigma-Aldrich) with protease inhibitor mixture (Nacalai Tesque, Kyoto, Japan) and phosphatase inhibitor mixture (Nacalai Tesque). Cell lysates were separated by sodium dodecyl sulfate–polyacrylamide gel electrophoresis and transferred to polyvinylidene difluoride membranes. The membranes were blotted by the SNAP i.d. Protein Detection System (Millipore, Billerica, Mass) following the manufacturer's protocol. The membranes were blocked with 0.02% skim milk (BD Bioscience) in Tris-buffered saline (pH 7.4) containing 0.05% Tween 20 (TBST) and then incubated with the appropriate antibodies in TBST containing 0.02% skim milk. After washing, the membranes were incubated with horseradish peroxidase–conjugated anti–rabbit or mouse IgG antibodies (IBL, Takasaki, Japan) in TBST containing 0.02% skim milk. The membranes were washed twice with TBST, and then immunoreactive bands were visualized using an ECL Plus Detection System (GE Healthcare, Uppsala, Sweden).

Cytotoxicity assay

Cell viability was determined by using Cytotoxity Detection Kit PULS (LDH) (Roche Diagnostics, Basel, Switzerland) following the manufacturer's protocol. As an apoptosis marker, caspase 3/7 activity was determined by the Caspase-Glo 3/7 assay (Promega, Madison, Wis) following the manufacturer's protocol.

Fluorescence immunostaining

To investigate the translocation of HMGB1, RAW-blue cells were cultured on Lab-Tek chamber slides (Nalge Nunc International, Cambridge, Mass) and incubated with each specimen for 24 h. Cells were then fixed with 4% paraformaldehyde for 15 min and permeabilized with 0.2% Triton X-100 in phosphate-buffered saline for 5 min. After washing with phosphate-buffered saline three times, cells were blocked in 5% sheep serum albumin in TBST for 1 h and incubated with rabbit anti-HMGB1 polyclonal antibody (SHINO-TEST) for 1 h at room temperature. The slides were then washed with TBST and incubated with anti–rabbit IgG conjugated with green Alexa Fluor 488 (Invitrogen, Carlsbad, Calif). Finally, the slides were covered by ProLong Gold with DAPI (Invitrogen). Images were captured using a fluorescence microscope (Keyence, Osaka, Japan).

Quantitative polymerase chain reaction

RAW-blue cells were stimulated with 5 mM of VPA for 24 h, and mRNA expression of γ-aminobutyric acid (GABA) receptors was analyzed by reverse transcriptase–polymerase chain reaction (RT-PCR). Total RNA from cells was purified with an RNeasy mini kit (Qiagen, Hombrechtikon, Switzerland) and DNdigest (Qiagen), and cDNA was synthesized using ReverTra Ace (Toyobo, Osaka, Japan) following the manufacturer's protocol. Real-time PCR was performed on a 7300 Real-time PCR System (Applied Biosystems, Carlsbad, Calif) using SYBR MIX Plus (Toyobo). The mouse HMGB1 transcript was amplified using the following primers: forward, 5′-CCA AAG GGG AGA CCA AAA AG-3′; reverse, 5′-TCA TAG GGC TGC TTG TCA TCT-3′. The mouse TNF-α transcript was amplified using the following primers: forward, 5′-AAG CCT GTA GCC CAC GTC GTA-3′; reverse, 5′-GGC ACC ACT AGT TGG TTG TCT TTG-3′. The mouse $GABA_A$ receptor subunit α1 transcript was amplified using the following primers: forward, 5′-CGA AGG TGG CTT ATG CAA CA-3′; reverse, 5′-CCC ACG CAT ACC CTC TCT TG-3′. The mouse $GABA_A$ receptor subunit α3 transcript was amplified using the following primers: forward, 5′-CTC CAA CAG CGA TTG CTT CA-3′; reverse, 5′-TGA TGC GGG AAA TTT TGT CA-3′. The mouse $GABA_A$ receptor subunit β2 transcript was amplified using the following primers: forward, 5′-AAC CGA GTG GCA GAC CAA CT-3′; reverse, 5′-TCG GGA TGC AAT CGA ATC AT-3′. Mouse β-actin transcript was used as an internal control: forward primer, 5′-CAT CCG TAA AGA CCT CTA TGC CAA-3′; reverse, 5′-ATG GAG CCA CCG ATC CAC-3′. The housekeeping gene, β-actin, was used to normalize all test genes, and data quantification was performed using the ΔΔCT method.

Murine model of endotoxemia

This study was approved and performed in accordance with the guidelines of the School of Dentistry, Aichi Gakuin University at Nagoya, Aichi, Japan. Endotoxemia was induced in Balb/c mice (male, 7–8 weeks old) by i.p. injection of *E. coli* LPS (1). Briefly, mice were injected s.c. with VPA (600 mg/kg) 12 h before LPS administration. The mice were monitored for survival over a period of 192 h after LPS administration. In some cases, VPA (600 mg/kg) with or without a neutralizing antibody for HMGB1 (2 or 4 mg/kg) was given to mice 12 h before LPS (25 mg/kg) administration. The mice were monitored for survival over a period of 192 h after LPS administration. In parallel experiments, blood was collected from mice at 24 h after LPS administration, and levels of serum IL-6 (kit purchased from IBL) and HMGB1 (kit purchased from SHINO-TEST) were determined by ELISA.

Statistics

Results are expressed as means ± SD. Mortality studies were analyzed using log-rank test. Statistical evaluation of the continuous data was performed by one-way analysis of variance, followed by Tukey test for between-group comparisons. These statistical analyses were done using the statistical software Statcel 2 (OMS Ltd., Saitama, Japan). The level of significance was considered to be $P < 0.05$.

RESULTS

VPA enhances systemic inflammatory responses induced by LPS in vivo and in vitro

To determine the effect of VPA on systemic inflammatory response *in vivo*, we used a mouse model of endotoxic shock induced by injecting purified *E. coli* LPS according to the modified method of Galanos et al. (20). Valproic acid was injected i.p. 12 h before administering saline or LPS, and the survival rate of the mice was determined. Fifty percent of the mice died within 3 days after administration of LPS (Fig. 1A). Valproic acid alone did not cause lethality in mice (Fig. 1A). However, pretreatment with VPA reduced the survival rate of

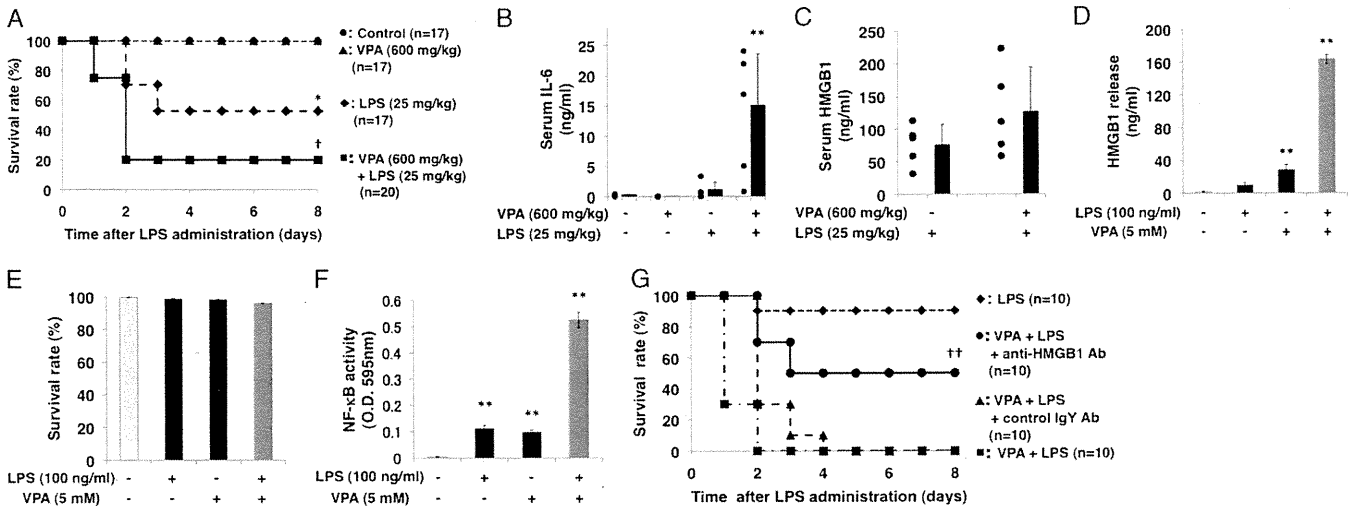

FIG. 1. **Valproic acid enhanced systemic inflammatory responses induced by LPS.** Valproic acid (600 mg/kg; s.c. injection) was given to mice 12 h before LPS administration (25 mg/kg; i.p. injection). Mice were monitored for survival over a period of 192 h after LPS administration (A) ($*P < 0.05$ vs. control, $^{\dagger}P < 0.05$ vs. LPS). Blood in mice was collected at 24 h after LPS administration, and levels of serum IL-6 and HMGB1 were determined by ELISA (B and C) ($**P < 0.01$ vs. control). RAW-blue cells were preincubated with VPA (5 mM) for 6 h and were then treated with LPS (100 ng/mL) for 24 h. The levels of HMGB1 in culture media were determined by ELISA (D) ($**P < 0.01$ vs. control). Cell viability was evaluated by LDH assay (E). Nuclear factor κB activity in RAW-blue cells was analyzed by a reporter assay, as described in Materials and Methods (F) ($**P < 0.01$ vs. control). Valproic acid (600 mg/kg) with or without a neutralizing chicken antibody for HMGB1 (4 mg/kg) and a control IgY antibody was given to mice 12 h before LPS (25 mg/kg) administration. Mice were monitored for survival over a period of 192 h after LPS administration (G) ($^{\dagger\dagger}P < 0.05$ vs. VPA + LPS).

mice (20%) (Fig. 1A). We also determined the concentrations of IL-6 and HMGB1 in serum of the mice. Serum was collected at 24 h after LPS administration, and levels of IL-6 and HMGB1 in the serum were determined by ELISA. Interleukin 6 was induced in serum in LPS-administered mice (Fig. 1B). Pretreatment with VPA significantly increased the concentration of IL-6 in serum in LPS-administered mice (Fig. 1B). Furthermore, serum levels of HMGB1 were increased in VPA-pretreated mice (Fig. 1C).

High-mobility group box 1 is a key mediator of systemic inflammation and sepsis (1). Therefore, we investigated whether VPA affects LPS-induced HMGB1 production in macrophages in culture. RAW-blue cells were preincubated with VPA (5 mM) for 6 h and were then treated with LPS (100 ng/mL) for 24 h. The levels of HMGB1 in culture media were detected by ELISA. Valproic acid as well as LPS induced HMGB1 release in macrophage cultures (Fig. 1D). However, release of HMGB1 significantly increased in cultures pretreated with VPA before stimulation with LPS (Fig. 1D). To exclude the possibility that HMGB1 in media leaks out from necrotic cells, we examined the effect of pretreatment of VPA and LPS stimuli on viability of macrophages. RAW-blue cells were preincubated with VPA (5 mM) for 6 h and were then treated with LPS (100 ng/mL) for 24 h. Cell viability was evaluated by LDH assay. Lipopolysaccharide or VPA alone or in combination did not affect the viability of macrophages (Fig. 1E). We next examined VPA activation of NF-κB in macrophage cultures. Pretreatment with VPA significantly enhanced LPS-induced NF-κB activation (Fig. 1F). To test the effect of HMGB1 blockade in the endotoxin shock mouse model, anti-HMGB1 chicken polyclonal antibodies or control IgY antibodies were injected into the peritoneal cavity simultaneously and after injection of VPA. All 10 mice in the group administered VPA and LPS were dead 2 days after LPS administration. However, when mice subjected to LPS administration were pretreated with anti-HMGB1 antibodies (total 4 mg/kg), 5 (50%) of the 10 mice survived for 8 days (Fig. 1G). In contrast, none of the 10 mice survived after pretreatment with VPA and control antibodies and then administration of LPS (Fig. 1G). These results suggest that VPA primes macrophages to respond to LPS and to produce inflammatory mediators such as HMGB1 and enhances systemic inflammatory responses in mice.

VPA induces HMGB1 release from macrophages

To confirm that VPA activates HMGB1 release, RAW-blue cells were incubated with VPA (5 mM), LPS (100 ng/mL), and TNF-α (20 ng/mL) for 24 h, and the amount of HMGB1 released into the medium was measured by ELISA. Valproic acid strongly induced HMGB1 in macrophage cultures, and the amounts of the protein released were comparable to those induced by *E. coli* LPS (Fig. 2A). Valproic acid–induced HMGB1 release increased time dependently and continued for up to 24 h (Fig. 2B). We next compared the localizations of HMGB1 in VPA-stimulated and nonstimulated macrophages. Strong nuclear localization of HMGB1 was observed in untreated macrophages, whereas nuclear-cytoplasmic translocation of HMGB1 was observed in macrophages stimulated with VPA, LPS, and TNF-α for 24 h (Fig. 2C). To determine whether VPA induces active HMGB1 release in the absence of cell death, the effects of VPA on cell viability were investigated by LDH assay. Valproic acid as well as LPS and TNF-α was not toxic to macrophages in culture (Fig. 2D). To determine the effect of VPA on the apoptosis pathway, we examined the activity of caspase 3/7 in VPA-treated macrophage cultures. Activity of caspase 3/7 was not increased by stimulation with VPA in macrophages (Fig. 2E). Moreover, VPA did not induce mRNA expression of HMGB1 in macrophages (Fig. 2F). We also examined mRNA expressions of HMGB1

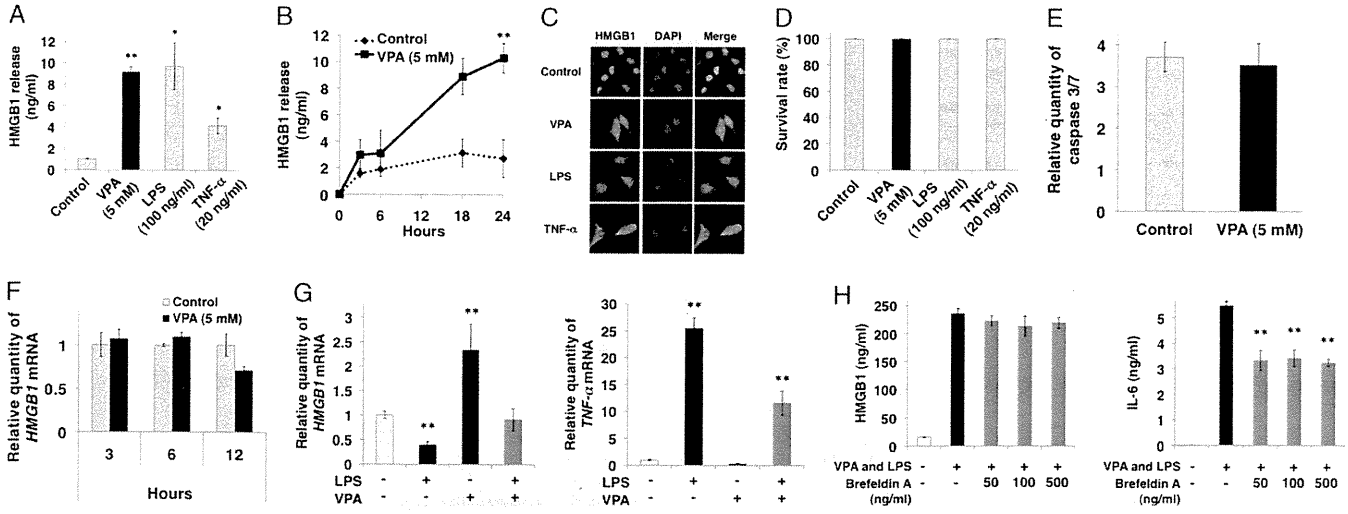

FIG. 2. **VPA induced HMGB1 release from macrophages.** RAW-blue cells were incubated with VPA (5 mM), LPS (100 ng/mL), and TNF-α (20 ng/mL) for 24 h (A). RAW-blue cells were incubated with VPA (5 mM) for 3, 6, 18, and 24 h (B). HMGB1 levels in supernatants were analyzed by ELISA (A and B). Translocation of HMGB1 in response to VPA (5 mM), LPS (100 ng/mL), and TNF-α (20 ng/mL) 24 h was analyzed by immunofluorescence assay (C). Cell viability was evaluated by LDH assay (D). Caspase 3/7 activity in the cells was analyzed by using a detection kit (E). Levels of *HMGB1* mRNA expresion were analyzed by real-time PCR and are shown as relative expression normalized by the levels of a housekeeping gene (*β-actin*) mRNA (F) (n = 3 ± SD, $*P < 0.05$ vs. control, $**P < 0.01$ vs. control). RAW-Blue cells were pre-incubated with Brefeldin A (50–500 ng/ml) for 3 h and were then treated with VPA (5 mM) and LPS (100 ng/ml) for 24 h. The levels of HMGB1 and IL-6 in culture media were determined by ELISA (H). (n = 3 ± S.D. $**P < 0.01$ vs. VPA and LPS).

and TNF-α by stimulations with LPS and VPA. Stimulation with VPA for 24 h increased steady-state levels of HMGB1 mRNA. However, LPS did not induce HMGB1 mRNA expression at a concentration of 100 ng/mL (Fig. 2G). High-mobility group box 1 mRNA levels also did not increase in RAW-blue cells primed with VPA and then stimulated with TNF-α. On the other hand, LPS strongly induced mRNA expression of TNF-α in RAW-blue cells (Fig. 2G). However, VPA did not induce its expression. These results suggest that HMGB1 release by stimulation with VPA due not to cell lysis or injury but to an active process that is not dependent on increase in gene expression and mRNA induction of HMGB1 by VPA is not due to activation of NF-κB. We also examined the effect of brefeldin A, a blocker of membrane export of proteins out of the endoplasmic reticulum, on release of HMGB1 induced by VPA and LPS. As shown in Figure 2H, the release of HMGB1 stimulated with VPA and LPS did not suppress by addition of brefeldin A, although the release of IL-6 stimulated with these stimulants suppressed with it at a concentration of 50 ng/ml. These results suggest that HMGB1 release with VPA and LPS were not due to the conventional secretory pathway.

ERK kinase may play a role in VPA-induced HMGB1 release

To clarify the mechanism by which VPA induces the release of HMGB1, we examined whether MAP kinases mediate VPA-induced HMGB1 release. Treatment of macrophages with VPA for 0.5 or 24 h activated phosphorylation of ERK (Fig. 3A). However, VPA did not induce phosphorylation of JNK and p38. In contrast, LPS induced phosphorylation of ERK, JNK, and p38. Inhibition of ERK with PD98059 suppressed VPA-induced ERK phosphorylation and HMGB1 release by macrophages (Fig. 3B and Supplemental Digital Content 5, at http://links.lww.com/SHK/A90). Valproic acid also induced NF-κB activation in macrophages (Fig. 3C), and it was inhibited by treatment with PD98059 (Fig. 3D). These findings suggest that VPA stimulates the release of HMGB1 from activated macrophages via ERK MAP kinase and NF-κB signaling. A recent study showed that acetylation of cytosolic HMGB1 triggers its exocytosis from monocytic cells (21).

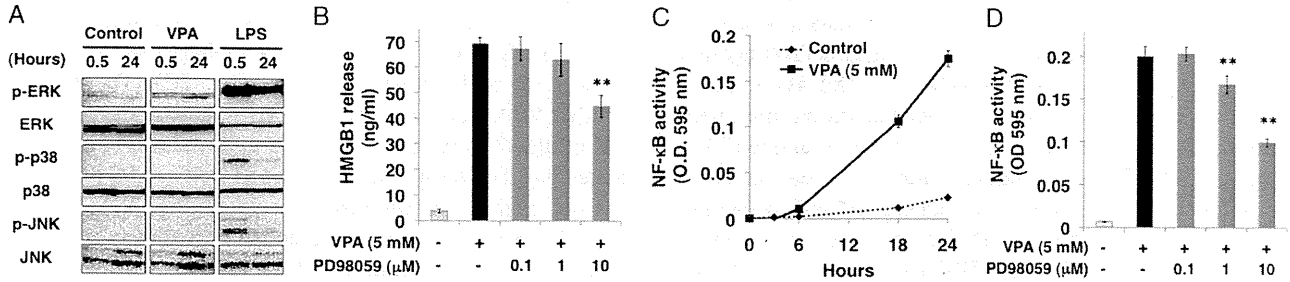

FIG. 3. **ERK kinase mediates VPA-induced HMGB1 release.** RAW-blue cells were incubated with VPA (5 mM) and LPS (100 ng/mL) for 0.5 to 24 h. Phosphorylation of p38MAPK, ERK1/2, and JNK was assayed by Western blot analysis (A). RAW-blue cells were incubated with VPA (5 mM) and PD98059 (0.1–10 μM) for 24 h. The levels of HMGB1 in culture supernatants were analyzed by ELISA (B). RAW-blue cells were incubated with VPA (5 mM) for 3, 6, 18, and 24 h (C). RAW-blue cells were incubated with VPA (5 mM) and PD98059 (0.1–10 μM) for 24 h (D). The levels of NF-κB activation were analyzed by reporter assay, as described in Materials and Methods (C and D) (n = 3 ± SD, $**P < 0.01$ vs. VPA).

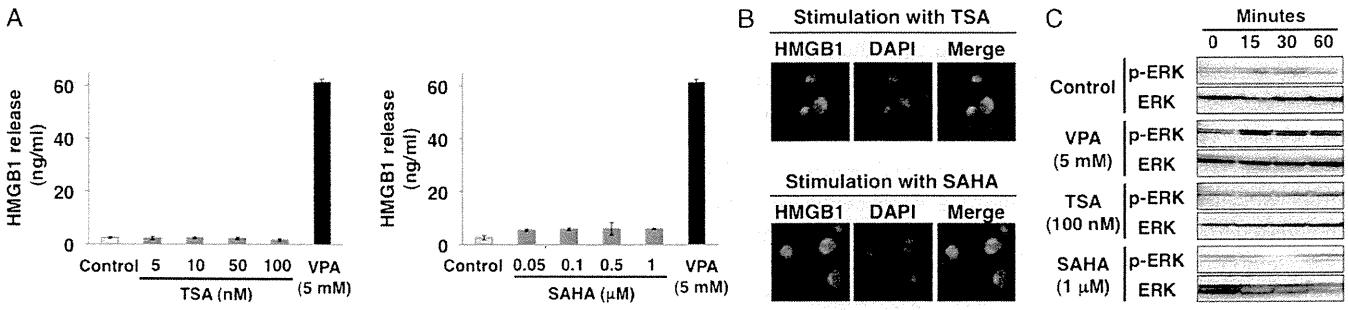

FIG. 4. **Histone deacetylases do not mediate the effects of VPA on HMGB1 release.** RAW-blue cells were incubated in histone deacetylase inhibitors TSA (5–100 nM) or SAHA (0.05–1 μM) for 24 h. The levels of HMGB1 in supernatants were evaluated by ELISA (A). Translocation of HMGB1 in response to TSA (100 nM) and SAHA (1 μM) for 24 h was analyzed by immunofluorescence assay (B). RAW-blue cells were incubated with VPA (5 mM), TSA (100 nM), and SAHA (1 μM) for 0 to 1 h. Phosphorylation of ERK1/2 was assayed by Western blot analysis (C) (n = 3 ± SD).

HDACs do not mediate the effects of VPA on HMGB1 release

Therefore, we examined the effects of TSA and SAHA, inhibitors of HDAC, on VPA-induced HMGB1 release in macrophage cultures. Trichostatin A and SAHA did not induce HMGB1 release from macrophages (Fig. 4A). In addition, HMGB1 was retained in nuclear regions, and the levels of HMGB1 in the cytoplasmic region were not increased after treatment with TSA and SAHA (Fig. 4B). Furthermore, TSA and SAHA did not activate phosphorylation of ERK, although VPA activated phosphorylation of ERK in the same conditions (Fig. 4C). These results suggest that VPA-induced HMGB1 release is not due to its inhibitory effect on HDACs.

VPA activates GABA signaling

Valproic acid exerts its antiepileptic effect principally by elevating GABA concentration in the brain (22, 23). Therefore, we next examined whether VPA increases GABA concentration in macrophage cultures. RAW-blue cells were stimulated with 5 mM of VPA for 24 h. γ-Aminobutyric acid levels in the cytoplasm and supernatants were analyzed by ELISA. Valproic acid induced GABA release into media (Figures 1A and B, Supplemental Digital Content 1, at http://links.lww.com/SHK/A85, and Supplemental Digital Content 2, at http://links.lww.com/SHK/A86). RAW cells were stimulated with VPA (5 mM) for 24 h. γ-Aminobutyric acid levels in supernatants (A) and cytoplasms (B) were analyzed by ELISA (n = 3 ± SD). We then confirmed that GABA release from macrophages acts on macrophages through a paracrine pathway and induces HMGB1 release. We examined the effect of GABA on HMGB1 release in macrophages. γ-Aminobutyric acid at concentrations of 1 to 1,000 μM did not activate the release of HMGB1 (Figures 2A and B, Supplemental Digital Content 3, at http://links.lww.com/SHK/A87, and Supplemental Digital Content 4, at http://links.lww.com/SHK/A88). RAW cells were stimulated with various concentrations (1–1,000 μM) of GABA for 24 h. High-mobility group box 1 levels in supernatants were analyzed by ELISA (A). Cell viability was evaluated by LDH assay (B) (n = 3 ± SD). These findings suggest that GABA did not mediate HMGB1 release induced by VPA.

Next, we examined whether VPA induces expression of GABA receptors in macrophages. RAW cells were stimulated with 5 mM of VPA for 24 h, and expression of $GABA_A$ receptor subunits in murine macrophages was investigated by quantitative RT-PCR. Among the α and β subunits, the β_2 subunit was expressed in macrophages (Fig. 5A). Expression of the α_1 and α_3 subunits of the $GABA_A$ receptor was induced by stimulation with 5 mM of VPA (Fig. 5A). Expression of α_2, α_4, α_5, and β_1 was not detected in macrophages with or without VPA stimulation (Fig. 5A). Picrotoxin, a $GABA_A$ receptor antagonist, inhibited VPA-induced HMGB1 release at a concentration of 0.5 μM (Fig. 5B). Picrotoxin also inhibited the activation of ERK phosphorylation by stimulation with VPA in macrophages (Fig. 5C). These results suggest that VPA induces HMGB1 release in macrophages in part through activation of $GABA_A$ receptors and ERK kinase.

DISCUSSION

In the present study, we demonstrated that VPA significantly augmented the proinflammatory response induced by

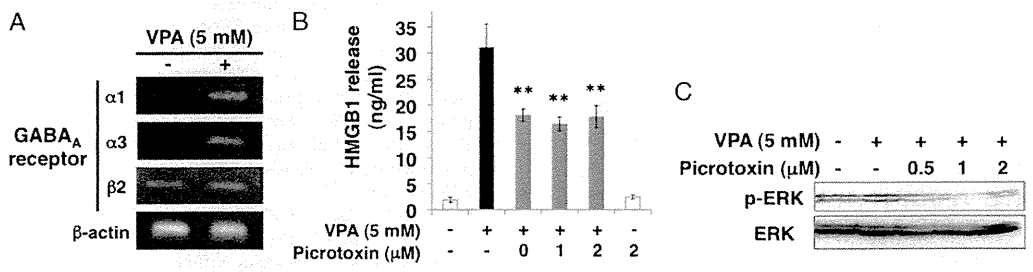

FIG. 5. **Valproic acid induced HMGB1 release by activating the $GABA_A$ receptor.** RAW-blue cells were stimulated with VPA (5 mM) for 24 h. Expression of $GABA_A$ receptor mRNA was analyzed by RT-PCR (A).RAW-blue cells were incubated with VPA (5 mM) in the presence or absence of picrotoxin (2 μM) for 24 h. The levels of HMGB1 in supernatants were analyzed by ELISA (B). Phosphorylation of ERK1/2 was detected by Western blot analysis (C) (n = 3 ± SD, $^{**}P < 0.01$ vs. VPA).

LPS both *in vivo* and *in vitro*. Valproic acid reduced survival in a mouse model of lethal endotoxemia by inducing HMGB1 release. Pharmacologic data show that VPA induces HMGB1 release through a pathway that might include GABA receptors and ERK MAP kinase.

A previous study demonstrated that HDAC inhibitors have broad anti-inflammatory properties via suppression of cytokine production (6, 24). These anti-inflammatory properties were demonstrated *in vitro* by inhibition of the secretion of proinflammatory cytokines in LPS- and cytokine-stimulated peripheral blood mononuclear cells (PBMCs) and in macrophages (6). Histone deacetylase inhibitors reduced circulating cytokine concentrations during endotoxemia in mice (25). Histone deacetylase inhibitors, by increasing the levels of histone acetylation, can lead to a local alteration in the structure of chromatin, which facilitates gene-specific repression of transcription. Therefore, HDAC inhibition is a relevant mechanism mediating anti-inflammatory effects.

How do HDACs and HDAC inhibitors regulate inflammation? Histone deacetylases were originally identified as enzymes that modify acetylation of histone proteins, thereby regulating gene expression. However, subsequent research has identified many other targets of acetylation, and acetylation of nonhistone proteins regulates a variety of other cell signaling pathways, including inflammation. Thus, at least three distinct pathways may exist for HDAC regulation of inflammation. First, HDACs might regulate gene expression of inflammatory mediators through modification of histone proteins. Second, HDACs might regulate transcription factors such as NF-κB that transactivate proinflammatory genes. Third, HDACs directly modify members of the mitogen-activated protein kinase (MAPK) pathway, such as MAPK phosphatase-1 (MKP-1), which in turn modulate transcription factors controlling innate immune responses (12).

Valproic acid is an HDAC inhibitor of the class of short-chain fatty acids, and it exhibited anti-inflammatory effects through histone hyperacetylation (16, 26). On the other hand, several mechanisms are known to promote the relocation of HMGB1 from the nucleus to cytoplasm, including the acetylation (21, 27) and phosphorylation (28) of HMGB1 and the destabilized association of HMGB1 with chromatin or a nuclear import protein (28). High-mobility group box 1 has been reported to be a substrate of histone acetylase, and it has been shown that HDAC inhibitors induce the relocation of HMGB1 from the nucleus to cytoplasm (21, 27). In this study, we demonstrated that VPA induced HMGB1 release in macrophage cultures and that the VPA-induced release of HMGB1 was not due to inhibition of HDAC (Fig. 4) or acetylation of HMGB1 (data not shown). However, VPA-induced HMGB1 release might be mediated in part through activation of GABA receptors and ERK MAP kinase. This conclusion is strengthened by our findings that inhibitors of ERK or GABA receptors abolished HMGB1 release stimulated by VPA. Phosphorylation of ERK is important for secretion of insulin (29) and various cytokines (30). Furthermore, the $GABA_A$ receptor regulates the phosphorylation of ERK. Therefore, our studies support the theory that MAPK signaling and GABA signaling mediate VPA activation of HMGB1 release.

High-mobility group box 1 is either secreted from activated monocytes and macrophages through secretory lysosomes (31) or passively leaked from cells when the integrity of the plasma membrane is disrupted during necrosis (32, 33). In this study, we demonstrated that VPA does not cause necrosis or apoptosis. These results suggested that VPA induced the release of HMGB1 through active exocytosis.

Gingival overgrowth is a common adverse effect of the administration of an antiepileptic drug such as VPA (19, 34). The presence of dental plaque is often associated with gingival overgrowth (35). Morphological changes in the gingiva lead to the retention of dental plaque. Bacterial components, such as LPS and lipoprotein, in dental plaque can be recognized by host cell Toll-like receptors and play an important role in the inflammatory response in periodontal tissue. Higher levels of HMGB1 were shown to be present in gingival crevicular fluid from periodontal patients (36). High-mobility group box 1 potentiates the action of LPS (37), and thus release of HMGB1 induced by VPA may exaggerate the outcome of bacterial insult in periodontal tissue.

REFERENCES

1. Wang H, Bloom O, Zhang M, Vishnubhakat JM, Ombrellino M, Che J, Frazier A, Yang H, Ivanova S, Borovikova L, et al.: HMG-1 as a late mediator of endotoxin lethality in mice. *Science* 285:248–251, 1999.
2. Gotfryd K, Skladchikova G, Lepekhin EA, Berezin V, Bock E, Walmod PS: Cell type–specific anti-cancer properties of valproic acid: independent effects on HDAC activity and Erk1/2 phosphorylation. *BMC Cancer* 10:383, 2010.
3. Zhu K, Qu D, Sakamoto T, Fukasawa I, Hayashi M, Inaba N: Telomerase expression and cell proliferation in ovarian cancer cells induced by histone deacetylase inhibitors. *Arch Gynecol Obstet* 277:15–19, 2008.
4. Duenas-Gonzalez A, Candelaria M, Perez-Plascencia C, Perez-Cardenas E, de la Cruz-Hernandez E, Herrera LA: Valproic acid as epigenetic cancer drug: preclinical, clinical and transcriptional effects on solid tumors. *Cancer Treat Rev* 34:206–222, 2008.
5. Hrzenjak A, Moinfar F, Kremser ML, Strohmeier B, Petru E, Zatloukal K, Denk H: Histone deacetylase inhibitor vorinostat suppresses the growth of uterine sarcomas *in vitro* and *in vivo*. *Mol Cancer* 9:49, 2010.
6. Halili MA, Andrews MR, Labzin LI, Schroder K, Matthias G, Cao C, Lovelace E, Reid RC, Le GT, Hume DA, et al.: Differential effects of selective HDAC inhibitors on macrophage inflammatory responses to the Toll-like receptor 4 agonist LPS. *J Leukoc Biol* 87:1103–1114, 2010.
7. Faraco G, Pittelli M, Cavone L, Fossati S, Porcu M, Mascagni P, Fossati G, Moroni F, Chiarugi A: Histone deacetylase (HDAC) inhibitors reduce the glial inflammatory response *in vitro* and *in vivo*. *Neurobiol Dis* 36:269–279, 2009.
8. Han SB, Lee JK: Anti-inflammatory effect of trichostatin-A on murine bone marrow-derived macrophages. *Arch Pharm Res* 32:613–624, 2009.
9. Kim HJ, Rowe M, Ren M, Hong JS, Chen PS, Chuang DM: Histone deacetylase inhibitors exhibit anti-inflammatory and neuroprotective effects in a rat permanent ischemic model of stroke: multiple mechanisms of action. *J Pharmacol Exp Ther* 321:892–901, 2007.
10. Reilly CM, Mishra N, Miller JM, Joshi D, Ruiz P, Richon VM, Marks PA, Gilkeson GS: Modulation of renal disease in MRL/lpr mice by suberoylanilide hydroxamic acid. *J Immunol* 173:4171–4178, 2004.
11. Leoni F, Zaliani A, Bertolini G, Porro G, Pagani P, Pozzi P, Dona G, Fossati G, Sozzani S, Azam T, et al.: The antitumor histone deacetylase inhibitor suberoylanilide hydroxamic acid exhibits antiinflammatory properties via suppression of cytokines. *Proc Natl Acad Sci U S A* 99:2995–3000, 2002.
12. Cao W, Bao C, Padalko E, Lowenstein CJ: Acetylation of mitogen-activated protein kinase phosphatase-1 inhibits Toll-like receptor signaling. *J Exp Med* 205:1491–1503, 2008.
13. Gottlicher M, Minucci S, Zhu P, Kramer OH, Schimpf A, Giavara S, Sleeman JP, Lo Coco F, Nervi C, Pelicci PG, et al.: Valproic acid defines a novel class of HDAC inhibitors inducing differentiation of transformed cells. *EMBO J* 20:6969–6978, 2001.
14. Herranz JL, Armijo JA, Arteaga R: Clinical side effects of phenobarbital, primidone, phenytoin, carbamazepine, and valproate during monotherapy in children. *Epilepsia* 29:794–804, 1988.

15. Blaheta RA, Cinatl J Jr: Anti-tumor mechanisms of valproate: a novel role for an old drug. *Med Res Rev* 22:492–511, 2002.
16. Ichiyama T, Okada K, Lipton JM, Matsubara T, Hayashi T, Furukawa S: Sodium valproate inhibits production of TNF-alpha and IL-6 and activation of NF-kappaB. *Brain Res* 857:246–251, 2000.
17. Garnier R, Boudignat O, Fournier PE: Valproate poisoning. *Lancet* 2:97, 1982.
18. El-Mowafy AM, Abdel-Dayem MA, Abdel-Aziz A, El-Azab MF, Said SA: Eicosapentaenoic acid ablates valproate-induced liver oxidative stress and cellular derangement without altering its clearance rate: dynamic synergy and therapeutic utility. *Biochim Biophys Acta* 1811:460–467, 2011.
19. Anderson HH, Rapley JW, Williams DR: Gingival overgrowth with valproic acid: a case report. *ASDC J Dent Child* 64:294–297, 1997.
20. Galanos C, Roppel J, Weckesser J, Rietschel ET, Mayer H: Biological activities of lipopolysaccharides and lipid A from Rhodospirillaceae. *Infect Immun* 16:407–412, 1977.
21. Bonaldi T, Talamo F, Scaffidi P, Ferrera D, Porto A, Bachi A, Rubartelli A, Agresti A, Bianchi ME: Monocytic cells hyperacetylate chromatin protein HMGB1 to redirect it towards secretion. *EMBO J* 22:5551–5560, 2003.
22. Nau H, Loscher W: Valproic acid: brain and plasma levels of the drug and its metabolites, anticonvulsant effects and gamma-aminobutyric acid (GABA) metabolism in the mouse. *J Pharmacol Exp Ther* 220:654–659, 1982.
23. Guidotti A, Auta J, Chen Y, Davis JM, Dong E, Gavin DP, Grayson DR, Matrisciano F, Pinna G, Satta R, et al.: Epigenetic GABAergic targets in schizophrenia and bipolar disorder. *Neuropharmacology* 60:1007–1016, 2011.
24. Halili MA, Andrews MR, Sweet MJ, Fairlie DP: Histone deacetylase inhibitors in inflammatory disease. *Curr Top Med Chem* 9:309–319, 2009.
25. Roger T, Lugrin J, Le Roy D, Goy G, Mombelli M, Koessler T, Ding XC, Chanson AL, Knaup Reymond M, Miconnet I, et al.: Histone deacetylase inhibitors impair innate immune responses to Toll-like receptor agonists and to infection. *Blood* 117:1205–1217, 2011.
26. Zhang Z, Zhang ZY, Fauser U, Schluesener HJ: Valproic acid attenuates inflammation in experimental autoimmune neuritis. *Cell Mol Life Sci* 65:4055–4065, 2008.
27. Carneiro VC, de Moraes Maciel R, de Abreu da Silva IC, da Costa RF, Paiva CN, Bozza MT, Fantappie MR: The extracellular release of *Schistosoma mansoni* HMGB1 nuclear protein is mediated by acetylation. *Biochem Biophys Res Commun* 390:1245–1249, 2009.
28. Youn JH, Shin JS: Nucleocytoplasmic shuttling of HMGB1 is regulated by phosphorylation that redirects it toward secretion. *J Immunol* 177:7889–7897, 2006.
29. Persaud SJ, Wheeler-Jones CP, Jones PM: The mitogen-activated protein kinase pathway in rat islets of Langerhans: studies on the regulation of insulin secretion. *Biochem J* 313:119–124, 1996.
30. Kawahara K, Biswas KK, Unoshima M, Ito T, Kikuchi K, Morimoto Y, Iwata M, Tancharoen S, Oyama Y, Takenouchi K, et al.: C-reactive protein induces high-mobility group box-1 protein release through activation of p38MAPK in macrophage RAW264.7 cells. *Cardiovasc Pathol* 17:129–138, 2008.
31. Gardella S, Andrei C, Ferrera D, Lotti LV, Torrisi MR, Bianchi ME, Rubartelli A: The nuclear protein HMGB1 is secreted by monocytes via a non-classical, vesicle-mediated secretory pathway. *EMBO Rep* 3:995–1001, 2002.
32. Scaffidi P, Misteli T, Bianchi ME: Release of chromatin protein HMGB1 by necrotic cells triggers inflammation. *Nature* 418:191–195, 2002.
33. Bianchi ME, Manfredi AA: High-mobility group box 1 (HMGB1) protein at the crossroads between innate and adaptive immunity. *Immunol Rev* 220:35–46, 2007.
34. Seymour RA, Smith DG, Turnbull DN: The effects of phenytoin and sodium valproate on the periodontal health of adult epileptic patients. *J Clin Periodontol* 12:413–419, 1985.
35. Seymour RA, Ellis JS, Thomason JM: Risk factors for drug-induced gingival overgrowth. *J Clin Periodontol* 27:217–223, 2000.
36. Morimoto Y, Kawahara KI, Tancharoen S, Kikuchi K, Matsuyama T, Hashiguchi T, Izumi Y, Maruyama I: Tumor necrosis factor-alpha stimulates gingival epithelial cells to release high mobility-group box 1. *J Periodontal Res* 43:76–83, 2008.
37. Qin YH, Dai SM, Tang GS, Zhang J, Ren D, Wang ZW, Shen Q: HMGB1 enhances the proinflammatory activity of lipopolysaccharide by promoting the phosphorylation of MAPK p38 through receptor for advanced glycation end products. *J Immunol* 183:6244–6250, 2009.

TISSUE ENGINEERING: Part A
Volume 17, Numbers 15 and 16, 2011

DOI: 10.1089/ten.tea.2010.0615

Complete Pulp Regeneration After Pulpectomy by Transplantation of CD105$^+$ Stem Cells with Stromal Cell-Derived Factor-1

Koichiro Iohara, Ph.D.,[1] Kiyomi Imabayashi, Ph.D.,[1] Ryo Ishizaka, D.D.S.,[1,2] Atsushi Watanabe, Ph.D.,[3] Junichi Nabekura, Ph.D.,[4] Masataka Ito, Ph.D.,[5] Kenji Matsushita, Ph.D.,[1] Hiroshi Nakamura, Ph.D.,[6] and Misako Nakashima, Ph.D.[1]

Loss of pulp due to caries and pulpitis leads to loss of teeth and reduced quality of life. Thus, there is an unmet need for regeneration of pulp. A promising approach is stem cell therapy. Autologous pulp stem/progenitor (CD105$^+$) cells were transplanted into a root canal with stromal cell-derived factor-1 (SDF-1) after pulpectomy in mature teeth with complete apical closure in dogs. The root canal was successfully filled with regenerated pulp including nerves and vasculature by day 14, followed by new dentin formation along the dentinal wall. The newly regenerated tissue was significantly larger in the transplantation of pulp CD105$^+$ cells with SDF-1 compared with those of adipose CD105$^+$ cells with SDF-1 or unfractionated total pulp cells with SDF-1. The pulp CD105$^+$ cells highly expressed angiogenic/neurotrophic factors compared with other cells and localized in the vicinity of newly formed capillaries after transplantation, demonstrating its potent trophic effects on neovascularization. Two-dimensional electrophoretic analyses and real-time reverse transcription–polymerase chain reaction analyses demonstrated that the qualitative and quantitative protein and mRNA expression patterns of the regenerated pulp were similar to those of normal pulp. Thus, this novel stem cell therapy is the first demonstration of complete pulp regeneration, implying novel treatment to preserve and save teeth.

Introduction

DENTAL PULP has many functions, and it is essential for longevity of teeth and quality of life. The long-term goal of endodontic treatment after deep caries and/or pulp inflammation is the conservation and restoration of teeth including dental pulp. A promising approach for it is stem-cell-based therapy to regenerate the dentin-pulp complex for the conservation and total restoration of structure and function.[1] The regeneration and tissue engineering of pulp is based on morphogens and growth factors, responding stem/progenitor cells, and the extracellular matrix scaffold.[2] The regeneration of dental pulp in immature teeth with incomplete apical closure has been reported using fibrin in the blood clot or collagen.[3,4] However, there have been no reports concerning total pulp regeneration in mature teeth with complete apical closure by stem/progenitor cell therapy. There is an intimate association of innervation with vasculature of the dental pulp. Angiogenesis/vasculogenesis and neurogenesis are critical for total functional pulp regeneration. The type III receptor of the transforming growth factor-β receptor family cell surface antigen CD105 (endoglin) was selected on the basis of its wide expression on mesenchymal stem cells (MSCs).[5] The stromal cell-derived factor-1 (SDF-1)/CXCR4 axis is present and functional in MSC populations.[6,7] CD105$^+$ stem/progenitor cells from human pulp tissue containing CXCR4-positive cells demonstrated angiogenic/vasculogenic and neurogenic potential.[8] Endothelial cells release SDF-1 under hypoxic conditions and promote cell survival and neovascularization by recruitment and perivascular retention of CXCR4-positive bone marrow-derived cells.[9,10] Therefore, in this study, autologous pulp CD105$^+$ cells were transplanted with SDF-1 in a collagen scaffold into the root canal of mature teeth induced complete apical closure after pulpectomy, in dogs. Thus, we demonstrate for the first time complete pulp regeneration in the root canal, by protein profiles and mRNA expression patterns.

[1]Department of Dental Regenerative Medicine, Center of Advanced Medicine for Dental and Oral Diseases, National Center for Geriatrics and Gerontology, Research Institute, Obu, Aichi, Japan.
[2]Department of Pediatric Dentistry, School of Dentistry, Aichi-gakuin University, Nagoya, Aichi, Japan.
[3]Department of Cognitive Brain Science, National Center for Geriatrics and Gerontology, Research Institute, Obu, Aichi, Japan.
[4]Department of Developmental Physiology, National Institute for Physiological Sciences, Okazaki, Aichi, Japan.
[5]Department of Developmental Anatomy and Regenerative Medicine, National Defense Medical College, Tokorozawa, Saitama, Japan.
[6]Department of Endodontology, School of Dentistry, Aichigakuin University, Nagoya, Aichi, Japan.

Materials and Methods

Cell isolation

Dental pulp cells were separated from pulp tissues of maxillary teeth in dogs as previously described.[11] Primary adipose cells were also separated from the adipose tissue of the same dog as a control. Those primary cells, $2–5 \times 10^5$ cells each were stained with anti-mouse IgG1 negative control (W3/25) (AbD Serotec), mouse IgG1 negative control (Phycoerythrin [PE]) (MCA928PE) (AbD Serotec), and mouse anti-human CD105 (PE) (43A3) (BioLegend), 10 μL per 10^6 cells for 90 min at 4°C, and were sorted by a flow cytometer JSAN (Bay Bioscience). Both $CD105^+$ cells and $CD105^-$ cells derived from the pulp and adipose tissue and total pulp cells without cell fractionation were cultured in EBM2 (Cambrex Bio Science) supplemented with 10 ng/mL IGF (Cambrex Bio Science), 5 ng/mL EGF (Cambrex Bio Science), and 10% FBS (Invitrogen Corporation) to maintain the cells. They were subcultured after reaching 60%–70% confluence.

The phenotype of pulp $CD105^+$ cells was further characterized by flowcytometry at the third passage of culture in comparison with adipose $CD105^+$ cells and unfractionated total pulp cells after immunolabeling with antigen surface markers (Supplementary Material; Supplementary Data are available online at www.liebertonline.com/tea). The experiments were repeated nine times.

Real-time reverse transcription-polymerase chain reaction analysis

To further characterize the phenotype of the cell populations, total RNA were extracted using Trizol (Invitrogen) from the pulp and adipose $CD105^+$ cells and total pulp cells at the third passage. The number of these cells was normalized to 5×10^4 cells in each experiment. First-strand cDNA syntheses were performed from total RNA by reverse transcription using the ReverTra Ace-α (Toyobo). Real-time reverse transcription–polymerase chain reaction (RT-PCR) amplifications were performed at 95°C for 10 s, 62°C for 15 s, and 72°C for 8 s using stem cell markers, canine *CXCR4, Sox2, Stat3, Bmi1, and Rex1* (Supplementary Table S1) labeled with Light Cycler-Fast Start DNA master SYBR Green I (Roche Diagnostics) in Light Cycler (Roche Diagnostics). The design of the oligonucleotide primers was based on published canine cDNA sequences. When canine sequences were not available, human sequences were used. To examine mRNA expression of angiogenic and neurotrophic factors, real-time RT-PCR amplifications of canine *matrix metalloproteinase-3 (MMP-3), VEGF-A, granulocyte-monocyte colony-stimulating factor (GM-CSF), SDF-1, nerve growth factor (NGF), brain-derived neurotrophic factor (BDNF), Neuropeptide Y, Neurotrophin 3, E-selectin, VCAM 1, rhombotin 2, ECSCR,* and *SLC6A6* were also performed (Supplementary Table S1). The RT-PCR products were confirmed by sequencing based on published cDNA sequences. The expression in pulp $CD105^+$ cells and adipose $CD105^+$ cells was compared with that in total pulp cells at the third passage of culture after normalizing with β-*actin*.

Induced differentiation

The differentiation of pulp $CD105^+$ cells from the third to fifth passage, into adipogenic, angiogenic, neurogenic, and odontogenic/osteogenic lineages, was determined and compared with adipose $CD105^+$ cells and unfractionated pulp cells as previously described.[12]

Proliferation and migration assay

To determine cell proliferation in response to SDF1 (Acris), pulp $CD105^+$ cells were compared with total pulp cells and adipose $CD105^+$ cells at fourth passage at the 10^3 cells per 96 well in EBM2 supplemented with 0.2% bovine serum albumin (Sigma) and SDF-1 (50 ng/mL). Ten microliters of Tetracolor one® (Seikagaku Kogyo) was added to the 96-well plate, and cell numbers were measured at 2, 12, 24, and 36 h of culture using a spectrophotometer at 450 nm absorbance. Wells without cells served as negative controls.

To examine migration activity of pulp $CD105^+$ cells by SDF-1, horizontal chemotaxis assay was performed and compared with total pulp cells and adipose $CD105^+$ cells. The TAXIScan-FL (Effector Cell Institute) was used to detect real-time horizontal chemotaxis of cells. The TAXIScan-FL consists of an etched silicon substrate and a flat glass plate, both of which form two compartments with a 6 μm deep microchannel. Each cell fraction (1 μL of 10^5cells/mL) was placed into the single hole with which the device is held together with a stainless steel holder, and 1 μL of 10 ng/μL of SDF-1 was placed into the contra-hole. The video images of cell migration were taken for 6 h.

In vivo *transplantation studies*

An experimental model of whole pulp removal and transplantation of cell populations for regeneration was established in the permanent teeth in dogs to achieve complete apical closure (Narc). The whole pulp removal was carried out in both sides of upper second incisors and lower third incisors under intravenously administered sodium pentobarbital (Schering-Plough) followed by enlargement of apical foramen, 0.7 mm in width using #70 K-file (MANI). Autologous transplantation of the pulp $CD105^+$ cells, adipose $CD105^+$ cells, or total pulp cells, 1×10^6cells in each, from the third to fourth passage, after DiI labeling was performed with collagen TE, a mixture of collagen type I and type III (Nitta Gelatin) in the lower part of the root canals. The upper part of the root canals was further filled with SDF-1 at the final concentration of 15 ng/μL, with collagen TE. The cavity was sealed with zinc phosphate cement (Elite Cement, GC) and composite resin (Clearfil FII) after treatment with a bonding agent (Clearfil Mega Bond). Sixty teeth from 15 dogs were used. Ten teeth transplanted with pulp $CD105^+$ cells with SDF-1, 5 teeth transplanted with adipose $CD105^+$ cells with SDF-1, 5 teeth transplanted with total pulp cells with SDF-1, 5 teeth with SDF-1 only without cells, 5 teeth with pulp $CD105^+$ cells only without SDF-1, and 5 teeth with a scaffold only without cells were harvested for histology after 14 days. Six teeth transplanted with pulp $CD105^+$ cells with SDF-1 were harvested for two-dimensional electrophoretic analyses after 28 days. Four teeth each transplanted with pulp $CD105^+$ cells with SDF-1, adipose $CD105^+$ cells with SDF-1, and total pulp cells with SDF-1 were harvested after 90 days, respectively. Seven normal teeth without any operation were used as control. For morphological analyses, they were fixed in 4% paraformaldehyde (Nakarai Tesque) at 4°C overnight and embedded in paraffin wax (Sigma) after demineralization with 10% formic acid. The paraffin sections

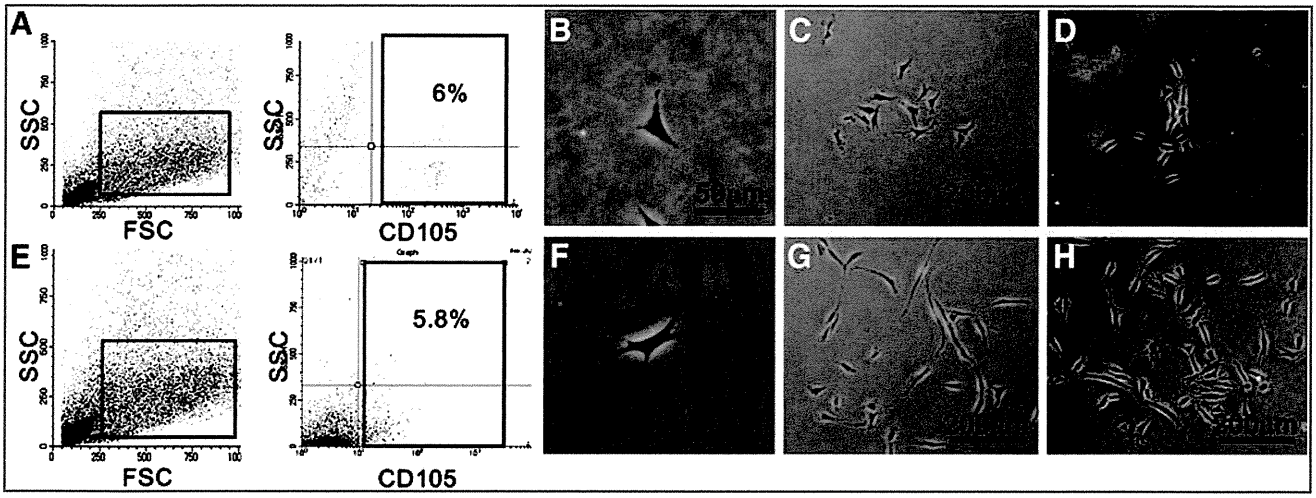

FIG. 1. Isolation of CD105$^+$ cells from adult canine dental pulp and adipose tissue. **(A)** The two panels show flow cytometry profiles of forward scatter (FSC) and side scatter (SSC) (left), and CD105 and SSC expression (right) on the dental pulp tissue. CD105$^+$ cells represented 6% of the total. **(B)** Primary pulp CD105$^+$ cell culture on day 3. **(C)** Primary pulp CD105$^+$ cell culture on day 10. **(D)** Primary total pulp cells on day 10. **(E)** The two panels show flow cytometry profiles of FSC and SSC (left), and CD105 and SSC expression (right) on the adipose tissue. CD105$^+$ cells represented 5.8% of the total. **(F)** Primary adipose CD105$^+$ cell culture on day 3. **(G)** Primary adipose CD105$^+$ cell culture on day 10. **(H)** Primary total adipose cells on day 10. The experiments were repeated nine times, and one represented experiment is presented. Color images available online at www.liebertonline.com/tea

(5 μm in thickness) were morphologically examined after staining with hematoxylin and eosin (HE).

All animal experiments were conducted using the strict guidelines of the Animal Protocol Committees and DNA Safety Programs both in National Center for Geriatrics and Gerontology and Aichigakuin University.

For vascular staining, 5-μm-thick paraffin sections stained with Fluorescein Griffonia (Bandeiraea) Simplicifolia Lectin 1/fluorescein-galanthus nivalis (snowdrop) lectin (20 μg/mL; Vector laboratories) for 15 min a fluorescence microscope BIOREVO, BZ-9000 (KEYENCE) were used.

For whole mount staining of vascular structure, the regenerated tissue and normal pulp tissue were dissected from teeth on day 14 and fixed in 4% paraformaldehyde for 45 min. The tissue was treated with 0.3% Triton X in phosphate-buffered saline, blocked, and stained with isolectin GS-IB4 from Griffonia simplicifolia, Alexa Fluor 488 conjugate (1:500) for 12 h at 4°C overnight. Neovascularization and engraftment of the transplanted cells into the root canal was examined by two-photon microscopy using FV1000MPE (Olympus) instrument. Three-dimensional structures were reconstructed by FV10-ASW software.

For neuronal staining, 5-μm-thick paraffin sections were incubated for 15 min with 0.3% Triton X-100 (Sigma Chemical). After incubation with 2.0% normal goat serum to block non-specific binding, they were incubated with goat anti-human PGP9.5 (Ultra Clone) (1:10000) at 4°C overnight. After three washes in phosphate-buffered saline, bound antibodies were reacted with biotinylated goat anti-rabbit IgG secondary antibody (Vector) (1:200) for 1 h at room temperature. The sections were also developed with the ABC reagent (Vector Laboratories), using the DAB chromogen for 10 min.

Relative amounts of regenerative pulp tissue 14 days after transplantation were examined in each sample by capturing video images of the histological preparations on the binocular microscopy (Leica, M 205 FA). Three sections at 150-μm intervals for each tooth from a total of 5 teeth each transplanted with pulp CD105$^+$ cells with SDF-1, adipose CD105$^+$ cells with SDF-1, total pulp cells with SDF-1, pulp CD105$^+$ cells only, SDF-1 only, and collagen TE scaffold only were examined. On-screen image outlines of newly regenerated pulp tissue and newly formed dentin were traced, and the surface area of these outlines in the root canal was determined by using Leica Application Suite software. The ratio of the regenerated area to the root canal area was calculated in three sections of each tooth, and the mean value was determined.

In vivo gene expression of odontoblastic differentiation markers, *dentin sialophosphoprotein* (*Dspp*) and *enamelysin*, in the cells lining along the root canal surface was examined by

TABLE 1. FLOW CYTOMETRIC ANALYSIS OF CELL-SURFACE MARKERS ON PULP AND ADIPOSE-DERIVED CD105$^+$ CELLS AND TOTAL PULP CELLS AT THE THIRD PASSAGE OF CULTURE

	Pulp CD105$^+$ cells	*Adipose CD105$^+$ cells*	*Total pulp cells*
CD24	1.8%	1.7%	0.3%
CD29	95.9%	90.5%	99.2%
CD31	0%	0%	0%
CD33	3.7%	0%	0.2%
CD34	45.5%	0.1%	47.1%
CD44	96.2%	92.3%	99.9%
CD73	97.2%	0.8%	22.3%
CD90	98.1%	95.6%	97.5%
CD105	98.5%	74.0%	4.6%
CD146	0.8%	0.2%	0.9%
CD150	2.3%	0.2%	0.9%
MHC class I	36.0%	80.0%	73.8%
MHC class II	0.4%	0%	0.4%
CXCR4	12.2%	5.9%	5.3%

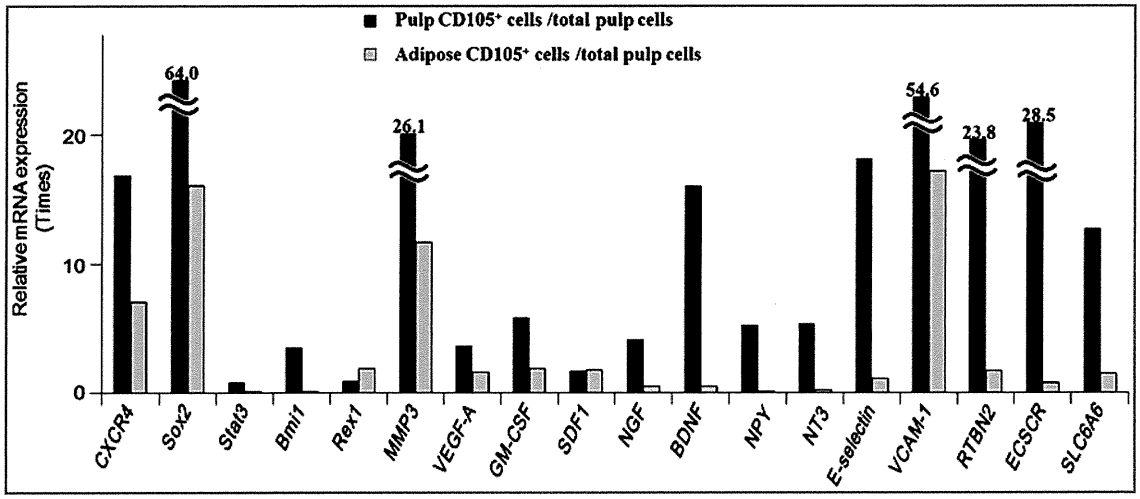

FIG. 2. Relative mRNA expression of cytokines of vasculogenesis and neurogenesis by real-time reverse transcription-polymerase chain reaction in pulp and adipose-derived CD105$^+$ cells. The experiments were repeated four times, and one represented experiment is presented.

in situ hybridization in 5 μm-paraffin sections 90 days after transplantation of pulp CD105$^+$ cells with SDF-1. Canine cDNA of *Dspp* (183 bp) and *enamelysin* (195 bp) linearized with *Nco*I and *Spe*I, respectively, were used as anti-sense probes. The probes were constructed out of the plasmids after subcloning the PCR products using the same primers as those designed for real-time RT-PCR (Supplementary Table S1). The DIG signals were detected by TSA system (PerkinElmer).

Two-dimensional electrophoretic analyses and gene expression analyses

For two-dimensional electrophoretic analysis, the regenerated pulp-like tissue on day 28, normal pulp, and periodontal ligament were homogenized in lysis buffer (6 M urea, 1.97 M thiourea, 2% [w/v] 3-[(3-cholamidopropyl) dimethylammonio] propanesulfonate, 64.8 mM dithiothreitol [DTT], 2% [v/v] Pharmalyte) and sonicated. The supernatant was collected after being centrifuged at 15,000 rpm for 15 min at 4°C, and applied to two-dimensional electrophoresis. Isoelectric focusing (IEF) was carried out using CoolPhoreSter 2-DE systems. IPG strips (Immobiline DryStrips, pH 4–7, 18 cm; GE) were used according to the manufacturer's instructions. IPG strips were rehydrated with rehydration solution (6 M urea, 1.97 M thiourea, 2% [v/v] TritonX-100, 13 mM DTT, 2% [v/v] Pharmalyte, 2.5 mM acetic acid, 0.0025% bromophenol blue [BPB]) overnight at 20°C. IEF was performed following a step-wise voltage incremental manner: 500 V for 2 h, 700–3000 V for 1 h, and 3500 V for 24 h. After IEF, IPG strips were incubated in an equilibration buffer (6 M urea, 32.4 mM DTT, 5 mM Tris-HCl, pH 6.8, 2% [w/v] sodium dodecyl sulfate [SDS], 0.0025% BPB, 30% [v/v] Glycerol) for 30 min. IPG strips were further equilibrated in 5 mM Tris-HCl, pH 6.8, 2% (w/v) SDS, 0.0025% BPB, 30% (v/v) Glycerol, and 243 mM iodoacetamid for 20 min. Separation in the second dimension was carried out in 12.5% SDS-PAGE gels (20 cm × 20 cm) at a constant current of 25 mA/gel for 15 min and 30 mA/gel thereafter. The gels were stained with Flamingo Fluorescent Gel Stain (Bio-Rad Laboratories) and scanned (FluoroPhorester 3000; Anatech). The gel images were analyzed and compared with each other by using Progenesis (Nonlinear Dynamics).

Real-time RT-PCR amplifications were performed as previously described using markers for periodontal ligament, canine *axin2*, *periostin*, and *asporin*/periodontal ligament-associated protein 1 (*PLAP-1*). *Collagen αI(I)*, *syndecan3*, and *tenascin C* were also used for comparison of regenerated tissue with normal pulp and periodontal ligament (Supplementary Table S1).

For microarray analysis, biotinylated cRNA were prepared from 250 ng of total RNA according to the standard Affymetrix protocol (Affymetrix Japan K.K.). After fragmentation, 10 μg of cRNA were hybridized for 16 h at 45°C on GeneChip Canine Genome 2.0 Array (Affymetrix) containing ~43,000 annotated sequences. GeneChips were washed and stained in the Affymetrix Fluidics Station 450, and were scanned using the Affymetrix GCS3000 scanner. The data were analyzed with Microarray Suite version 5.0 (MAS 5.0) using Affymetrix default analysis settings and global scaling as normalization method. The trimmed mean target intensity of each array was set to 500. Chips were ordered into hierarchical clusters using the Pearson centered algorithm as the distance measure, and the Average algorithm as the linkage method.

Statistical analyses

Data are reported as means ± standard deviation. *p*-Values were calculated by using the unpaired Student's *t*-test. The number of replicates in each experiment is indicated in the figure legends.

Results

Isolation and characterization of CD105$^+$ cells from pulp and adipose tissue

Flow cytometric isolation of the CD105$^+$ cells from canine adult total pulp cells (Fig. 1D) was performed using antibodies against CD105. CD105$^+$ cells isolated from total adipose cells (Fig. 1H) of the same dog and unfractionated total pulp cells were used as controls. The pulp and adipose

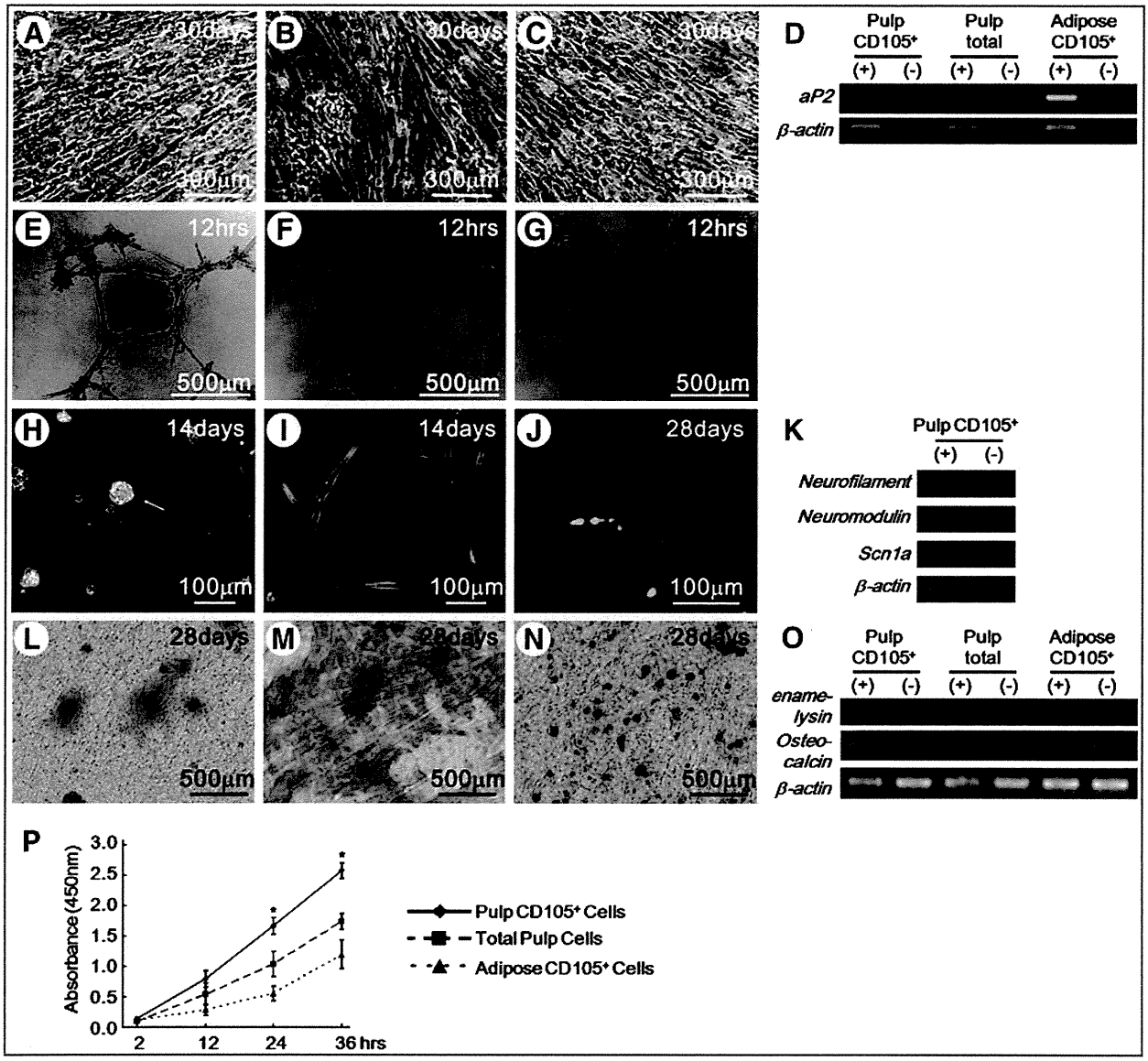

FIG. 3. Multi-lineage differentiation potential. **(A–D)** Adipogenic potential, **(E–G)** Angiogenic potential, **(H, I),** and Neurosphere formation. **(J)** Immunostaining with neurofilament. **(D)** *Adipocyte fatty acid binding protein 2 (aP2)* mRNA expression. **(K)** *Neurofilament, neuromodulin,* and *sodium channel, voltage-gated, type Ia (Scn1A)* mRNA expression. **(L–O)** Odontogenic/osteogenic potential. **(O)** Enamelysin and osteocalcin mRNA expression. **(A–C)** Oil red O staining. **(L–N)** Alizarin red staining. **(A, E, H, J, L)** Pulp $CD105^+$ cells. **(B, F, I, M)** Total pulp cells. **(C, G, N)** Adipose $CD105^+$ cells. **(P)** The proliferation activity of pulp $CD105^+$ cells, total pulp cells, and adipose $CD105^+$ cells with stromal cell-derived factor-1 (SDF-1). Data are expressed as means ± standard deviation of four determinations ($^*p < 0.01$). The experiments were repeated thrice, and one representative experiment is presented. Color images available online at www.liebertonline.com/tea

$CD105^+$ cells represented 6% and 5.8% of total cells, respectively (Fig. 1A, E). The $CD105^+$ cells from both the pulp and the adipose tissue were stellate with long cell processes (Fig. 1B, C, F, G). The pulp $CD105^-$ cells were of varied shapes with short processes. EBM2 supplemented with IGF1, EGF, and 10% FBS maintained the phenotype of $CD105^+$ cells, demonstrating more than 98% at the sixth passage. When single $CD105^+$ cells were plated in 35 mm dishes coated with type I collagen, they formed colonies in 10 days. This demonstrates the colony formation ability of these CD 105^+ cells. The efficiency of attachment and growth of pulp 105^+, adipose $CD105^+$, and pulp $CD105^-$ cells was estimated to be 8%, 3.7%, and 1%, respectively. Limiting dilution analysis at the third passage culture showed that the frequency of CFU in pulp $CD105^+$ cells was estimated to be 80%, whereas that in total pulp cells was 30%, and that in adipose $CD105^+$ cells was 50%.

To characterize the "stemness" of pulp $CD105^+$ cells, cell surface antigen markers were examined by flow cytometry and compared with adipose $CD105^+$ cells and total pulp cells. Pulp $CD105^+$ cells, adipose $CD105^+$ cells, and total pulp cells were positive for CD29, CD44, CD90, and CD105 and negative for CD31 at the third passage, which are minimal criteria for MSCs. It is noteworthy that the percentages of pulp $CD105^+$ cells which expressed CD73, CD150, and CXCR4 were much higher compared with adipose $CD105^+$

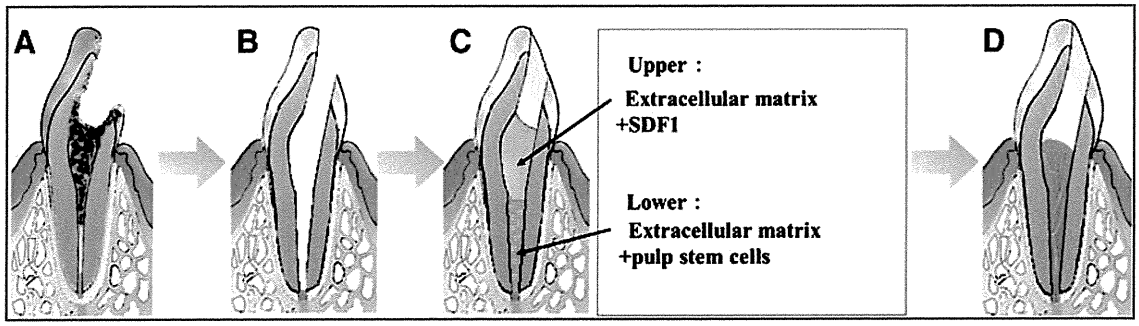

FIG. 4. Schematic diagrams of a canine model for complete pulp regeneration in permanent mature teeth. **(A)** pulpitis model, **(B)** whole pulp removal, and enlargement of apical foramen, 0.7 mm in width, **(C)** irrigation and filling with stem/progenitor cells in the lower part and SDF-1 in the upper part of the root canal together with collagen scaffold, **(D)** complete pulp regeneration. Color images available online at www.liebertonline.com/tea

cells and total pulp cells (Table 1). The expression of stem cell markers, *CXCR4, Sox2, and Bmi1* mRNA, was 16.8, 64, and 3.5 times higher in pulp CD105$^+$ cells than those in total pulp cells, respectively, suggesting the stem cell properties of pulp CD105$^+$ cells. Further, the pulp-derived CD105$^+$ cells exhibited higher expression of the characteristic stem cell markers compared with the adipose-derived CD105$^+$ cells. Angiogenic factors and/or neurotrophic factors, *VEGF-A, GM-CSF, NGF, BDNF, neuropeptide Y, neurotrophin 3, E-selectin,* and *VCAM-1,* were expressed higher in pulp CD105$^+$ cells compared with total pulp cells and adipose CD105$^+$ cells (Fig. 2).

The differentiation of pulp CD105$^+$ cells into adipose cells (Fig. 3A, D), endothelial cells (Fig. 3E), neuronal cells (Fig. 3H, J, K), and odontoblast/osteoblast lineage (Fig. 3L, O) was observed. However, the mineralized matrix was higher in total pulp cells (Fig. 3M) than that in pulp CD105$^+$ cells (Fig. 3L). Adipose CD105$^+$ cells demonstrated adipogenic (Fig. 3C, D) and osteogenic potential (Fig. 3N, O) but neither angiogenic (Fig. 3G) nor neurogenic potential. The proliferation activity with SDF-1 was higher in pulp CD105$^+$ cells than that in total pulp cells and adipose CD105$^+$ cells (Fig. 3P). The migration activity with SDF-1 shown in the TAXIScan-FL was much higher in pulp CD105$^+$ cells compared with total pulp cells and adipose CD105$^+$ cells (Supplementary Videos A–C).

Pulp regeneration after transplantation of pulp CD105$^+$ cells in the root canal

We next demonstrated by the *in vivo* transplantation of autologous pulp CD105$^+$ cells with SDF-1 into the root canal of mature teeth induced complete apical closure after pulpectomy in dogs (Fig. 4). Pulp CD105$^+$ cells formed pulp-like tissue by day 14 when transplanted with SDF-1 (Fig. 5A–C). However, transplantation of CD105$^+$ cells alone (Fig. 5E), or SDF-1 alone (Fig. 5F), yielded less pulp. Statistical analysis showed that the regenerated area was significantly larger (3.3-fold and 4.2-fold increase) when pulp CD105$^+$ cells were transplanted with SDF-1 compared with CD105$^+$ cells alone or SDF-1 alone, respectively (Fig. 6). The odontoblast-like cells attached to the dentinal wall in the root canal, extending their processes into dentin tubules (Fig. 5D). The pulp-like tissue was further extended to the cementum-enamel junction under the cement filling 90 days after transplantation of pulp CD105$^+$ cells together with SDF-1 (Fig. 5G). The cells in the upper part of the regenerated tissue were spindle shaped (Fig. 5H), and those in the middle part were stellate-like (Fig. 5I) similar to those in the normal pulp (Fig. 5J). It is noteworthy that tubular dentin was observed along the dentinal wall (Fig. 5G, K). The odontoblasts lining the dentinal wall were positive for *enamelysin/MMP-20* (Fig. 5L) and *Dspp* (Fig. 5M), two markers for odontoblasts. However, if unfractionated total pulp cells are transplanted instead of CD105$^+$ cells, less tissue was observed (Fig. 5N, O), followed by evidence of mineralization on day 90 (Fig. 5Q, R). Similarly, when adipose tissue-derived CD105$^+$ cells were transplanted, much less regenerate tissue was observed (Fig. 5P). Further statistical analysis showed that the ratio of newly regenerated tissue to root canal surface area was significantly larger (51.6-fold and 2.2-fold increase) in the case of pulp CD105$^+$ cell transplantation with SDF-1 than in the case of transplantation of adipose CD105$^+$ cells with SDF-1 or total pulp cells with SDF-1 on day 14 (Fig. 6). Confocal laser microscopic analysis after staining with BS-1 lectin of cryosections demonstrated neovascularization in the regenerated tissue (Fig. 7A). Two-photon microscopic analysis showed that numerous DiI-labeled transplanted pulp CD105$^+$ cells were in the vicinity of the newly formed capillaries (Fig. 7B), implicating a trophic role for these cells in neovascularization. The three-dimensional image of induced vascularization in the regenerated tissue on day 14 (Fig. 7D) was similar in density and orientation to that in the normal pulp (Fig. 7E). The transplanted CD105$^+$ cells were observed overall in the newly regenerated pulp (Fig. 7C), suggesting their potential capacity to migrate to the upper site by SDF-1. The neuronal process stained by PGP9.5 antibody was extended into the newly regenerated pulp from apical foramen (Fig. 7F). DiI labeling on the regenerated pulp in the lower third incisor *in vivo* showed the neuronal process from regenerated pulp connecting to inferior alveolar nerve (Fig. 7G).

Two-dimensional electrophoretic protein analyses and gene expression analyses of pulp regeneration

Two-dimensional electrophoretic analyses demonstrated that the qualitative and quantitative protein pattern of regenerated pulp tissue on day 28 was similar to that of normal pulp tissue derived from the same individual. The protein spots detected both in normal and regenerated pulp tissue represented 85.5% (123 spots) (Supplementary Fig. S1A–C). On the other hand, there were some differences in the protein